Optical properties and sub-bandgap formation of nano-crystalline Si quantum dots embedded ZnO thin film

Kuang-Yang Kuo,[1] Shu-Wei Hsu,[1] Pin-Ruei Huang,[2] Wen-Ling Chuang,[1] Chuan-Cheng Liu,[1] and Po-Tsung Lee[1,2,*]

[1]Department of Photonics & Institute of Electro-Optical Engineering, National Chiao Tung University, 1001 Ta-Hsueh Road, Hsinchu 30010, Taiwan
[2]Department of Photonics & Display Institute, National Chiao Tung University, 1001 Ta Hsueh Road, Hsinchu 30010, Taiwan
*potsung@mail.NCTU.edu.tw

Abstract: In this study, we fabricate ZnO thin films with nano-crystalline Si (nc-Si) quantum dots (QDs) using a ZnO/Si multilayer deposition structure and a post-annealing process, and the formation of high crystallinity of Si QDs embedded in the crystalline ZnO matrix is demonstrated. For optical properties, the essential features of ZnO material, high transmission in long-wavelength and high absorption in short-wavelength ranges, are preserved. We observe significantly enhanced light absorption and an unusual photoluminescence emission peak contributed from the nc-Si QDs in the middle-wavelength range. In addition, we confirm the formation of optical sub-bandgap and the obtained value is quite close to the unusual PL emission peak. We show that meaningful sub-bandgap can form in ZnO thin film by embedding nc-Si QDs while maintaining the advantageous properties of ZnO matrix. This newly developed composite material, nc-Si QD embedded ZnO thin films, can be useful for various electro-optical applications.

References and links

1. B. H. Lai, C. H. Cheng, and G. R. Lin, "Multicolor ITO/SiO$_x$/p-Si/Al light emitting diodes with improved emission efficiency by small Si quantum dots," IEEE J. Quantum Electron. **47**(5), 698–704 (2011).
2. J. M. Shieh, W. C. Yu, J. Y. Huang, C. K. Wang, B. T. Dai, H. Y. Jhan, C. W. Hsu, H. C. Kuo, F. L. Yang, and C. L. Pan, "Near-infrared silicon quantum dots metal-oxide-semiconductor field-effect transistor photodetector," Appl. Phys. Lett. **94**(24), 241108 (2009).
3. E. C. Cho, S. Park, X. Hao, D. Song, G. Conibeer, S. C. Park, and M. A. Green, "Silicon quantum dot/crystalline silicon solar cells," Nanotechnology **19**(24), 245201 (2008).
4. Ü. Özgür, Y. I. Alivov, C. Liu, A. Teke, M. A. Reshnikov, S. Doğan, V. Avrutin, S.-J. Cho, and H. Morkoç, "A comprehensive review of ZnO materials and devices," J. Appl. Phys. **98**(4), 041301 (2005).
5. F. Sun, C. X. Shan, B. H. Li, Z. Z. Zhang, D. Z. Shen, Z. Y. Zhang, and D. Fan, "A reproducible route to p-ZnO films and their application in light-emitting devices," Opt. Lett. **36**(4), 499–501 (2011).
6. K. S. Leschkies, T. J. Beatty, M. S. Kang, D. J. Norris, and E. S. Aydil, "Solar cells based on junctions between colloidal PbSe nanocrystals and thin ZnO films," ACS Nano **3**(11), 3638–3648 (2009).
7. S.-H. K. Park, C.-S. Hwang, M. Ryu, S. Yang, C. Byun, J. Shin, J.-I. Lee, K. Lee, M. S. Oh, and S. Im, "Transparent and photo-stable ZnO thin-film transistors to drive an active matrix organic-light-emitting-diode display panel," Adv. Mater. (Deerfield Beach Fla.) **21**(6), 678–682 (2009).
8. Q. Cheng, E. Tam, S. Xu, and K. K. Ostrikov, "Si quantum dots embedded in an amorphous SiC matrix: nanophase control by non-equilibrium plasma hydrogenation," Nanoscale **2**(4), 594–600 (2010).
9. G. Faraci, S. Gibilisco, P. Russo, A. R. Pennisi, G. Compagnini, S. Battiato, R. Puglisi, and S. La Rosa, "Si/SiO$_2$ core shell clusters probed by Raman spectroscopy," Eur. Phys. J. B **46**(4), 457–461 (2005).
10. K. A. Alim, V. A. Fonoberov, and A. A. Balandin, "Origin of the optical phonon frequency shifts in ZnO quantum dots," Appl. Phys. Lett. **86**(5), 053103 (2005).
11. G. Viera, S. Huet, and L. Boufendi, "Crystal size and temperature measurements in nanostructured silicon using Raman spectroscopy," J. Appl. Phys. **90**(8), 4175–4183 (2001).

12. J. B. You, X. W. Zhang, Y. M. Fan, Z. G. Yin, P. F. Cai, and N. F. Chen, "Effect of deposition conditions on optical and electrical properties of ZnO films prepared by pulsed laser deposition," Appl. Surf. Sci. **197–198**, 363–367 (2002).
13. E.-C. Cho, M. A. Green, G. Conibeer, D. Song, Y.-H. Cho, G. Scardera, S. Huang, S. Park, X. J. Hao, Y. Huang, and L. V. Dao, "Silicon quantum dots in a dielectric matrix for all-silicon tandem solar cells," Adv. Optoelectron. **2007**, 69578 (2007).
14. D.-H. Kim, H. Jeon, G. Kim, S. Hwangboe, V. P. Verma, W. Choi, and M. Jeon, "Comparison of the optical properties of undoped and Ga-doped ZnO thin films deposited using RF magnetron sputtering at room temperature," Opt. Commun. **281**(8), 2120–2125 (2008).
15. Y. G. Wang, S. P. Lau, H. W. Lee, S. F. Yu, B. K. Tay, X. H. Zhang, and H. H. Hng, "Photoluminescence study of ZnO films prepared by thermal oxidation of Zn metallic films in air," J. Appl. Phys. **94**(1), 354–358 (2003).
16. S. Fujihara, Y. Ogawa, and A. Kasai, "Tunable visible photoluminescence from ZnO thin films through Mg-doping and annealing," Chem. Mater. **16**(15), 2965–2968 (2004).
17. C. Meier, A. Gondorf, S. Lüttjohann, A. Lorke, and H. Wiggers, "Silicon nanoparticles: Absorption, emission, and the nature of the electronic bandgap," J. Appl. Phys. **101**(10), 103112 (2007).
18. X. X. Wang, J. G. Zhang, L. Ding, B. W. Cheng, W. K. Ge, J. Z. Yu, and Q. M. Wang, "Origin and evolution of photoluminescence from Si nanocrystals embedded in a SiO₂ matrix," Phys. Rev. B **72**(19), 195313 (2005).
19. X. Wen, L. V. Dao, P. Hannaford, E.-C. Cho, Y. H. Cho, and M. A. Green, "Excitation dependence of photoluminescence in silicon quantum dots," New J. Phys. **9**(9), 337 (2007).
20. Y. C. Liu, S. K. Tung, and J. H. Hsieh, "Influence of annealing on optical properties and surface structure of ZnO thin films," J. Cryst. Growth **287**(1), 105–111 (2006).
21. Y.-P. Chan, J.-H. Lin, C.-C. Hsu, and W.-F. Hsieh, "Near-resonant high order nonlinear absorption of ZnO thin films," Opt. Express **16**(24), 19900–19908 (2008).
22. Z. Ma, X. Liao, G. Kong, and J. Chu, "Absorption spectra of nanocrystalline silicon embedded in SiO₂ matrix," Appl. Phys. Lett. **75**(13), 1857–1859 (1999).
23. S. Mirabella, R. Agosta, G. Franzò, I. Crupi, M. Miritello, R. Lo Savio, M. A. Di Stefano, S. Di Marco, F. Simone, and A. Terrasi, "Light absorption in silicon quantum dots embedded in silica," J. Appl. Phys. **106**(10), 103505 (2009).
24. L.-W. Lai and C.-T. Lee, "Investigation of optical and electrical properties of ZnO thin films," Mater. Chem. Phys. **110**(2–3), 393–396 (2008).

1. Introduction

Nano-crystalline silicon (nc-Si) quantum dots (QDs) embedded in Si-based dielectric materials like SiO_2 and Si_3N_4 had been extensively studied and integrated with various electro-optical devices, e.g. light emitting devices (LEDs) [1], transistors [2], photovoltaic (PV) cells [3], and so on. They exhibit the feasibility and show great potential for devices integrating nc-Si QDs. In this work, we embed nc-Si QDs into ZnO thin films because ZnO has many desirable features to function as nc-Si QDs' matrix material, such as wide and direct bandgap, high transparency, and highly tunable electrical properties [4]. So far, only few materials can simultaneously possess these properties. Hence, ZnO can serve as the nc-Si QDs' matrix material for bandgap engineering, efficiently avoid the visible and near-infrared light absorption, and decrease carrier's transportation loss from matrix to enhance the performance of electro-optical devices with nc-Si QDs. ZnO itself is also widely applied to a variety of applications like LEDs [5], PV cells [6], and transistors [7] and shows superior results. Undoubtedly, there are many advantages to embed nc-Si QDs in ZnO thin films. Therefore, it is important to demonstrate its fabrication feasibility and understand its optical properties. In this study, we fabricate the ZnO thin films with nc-Si QDs using a ZnO/Si multilayer (ML) structure by sputtering and a post-annealing process. The nano-structural, crystalline, and optical properties of ZnO thin films with nc-Si QDs are investigated and discussed.

2. Experiment

The ZnO/Si ML thin films with 20-bilayers were deposited on Si(100) wafers or fused quartzes at room-temperature by radio-frequency (RF) magnetron sputtering method. The sputtering powers of ZnO and Si are fixed at 75 W and 110 W, and the effective thicknesses of each ZnO and Si layers are fixed at 5 and 3 nm respectively. After deposition, the ZnO/Si ML thin films were annealed in N_2 environment for 5 minutes by furnace under different annealing temperatures from 700°C (FA-700) to 1000°C (FA-1000) with 100°C increment for the investigation on Si QDs formation with high crystallinity. For the post-annealing process, when the set temperature is arrived, the as-deposited samples were quickly put into, stayed for

5 minutes, and quickly taken out the furnace. The surface morphologies were analyzed by a Digital Instrument D3100 atomic force microscope (AFM). The high-resolution transmission electron microscope (HRTEM) images were observed by a JEOL JEM-2010F transmission electron microscope. The X-ray diffraction (XRD) patterns were examined by a Bede-D1 X-ray diffractometer with Cu K_α radiation. The Raman and photoluminescence (PL) spectra were measured using a 488 nm diode-pumped solid-state laser (Horiba LabRam HR). The transmission and reflection spectra were obtained by a UV-VIS-NIR spectrophotometer (Hitachi U-4100).

3. Results and discussions

In order to know the growth morphology of the sputtered Si atoms during deposition, Fig. 1 shows the tapping mode AFM images before and after depositing the Si layer with effective thickness of 3 nm on ZnO thin-layer. The clear formation of amorphous Si (a-Si) nano-clusters with maximum height of 5 nm and the much larger root-mean-square (RMS) surface roughness than that of ZnO thin-layer are clearly observed in the ZnO/Si single-bilayer. The density of nano-clusters is estimated to be ~2.4×10^{10} cm^{-2}. Similar results are also obtained from the ZnO/Si double-bilayers. It indicates that the sputtered Si atoms on ZnO thin-layer can self-aggregate to form a-Si nano-clusters, which will make the nc-Si QDs formation easier during annealing.
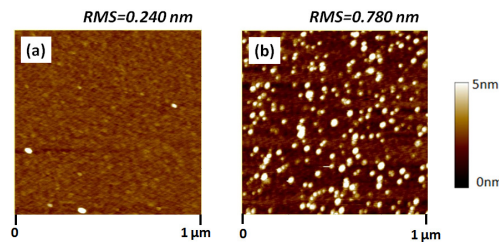

Fig. 1. AFM images of the as-deposited (a) ZnO thin-layer and (b) ZnO/Si single-bilayer.

Raman spectrum measurement, a reliable technique for examining the crystalline properties of nano-scaled Si materials [8, 9], is utilized to confirm the nc-Si QDs formation in ZnO thin films after annealing. The curve-fitting result of Raman spectrum for sample FA-1000 is shown in Fig. 2(a). In addition to the transverse optical (TO) modes of Si-Si vibrations in the a-Si, intermediate Si (i-Si), and nc-Si phases located at 480.0, 504.6, and 513.2 cm^{-1}, which are usually observed in the nc-Si QD thin films [8], the contribution of E_2(high) mode of ZnO matrix located at 436.2 cm^{-1} is also taken into account in this curve-fitting process [10]. The signal of i-Si phase comes from the grain boundaries or smaller crystallites [8]. The fitting curve composed of these four components shows an excellent match with the experimental data and an obvious nc-Si signal. Raman spectra of the ZnO/Si ML thin films under different annealing temperatures are shown in Fig. 2(b). The intensity of nc-Si significantly increases with increasing annealing temperature while that of a-Si decreases. The parameters of the curve-fitting results in Raman spectra for nc-Si and the calculated crystalline volume fraction of Si (f_c), where f_c is estimated from $(I_{i-Si} + I_{nc-Si})/(I_{a-Si} + I_{i-Si} + I_{nc-Si}) \times 100\%$ [8], are listed in Table 1. Sample FA-1000 shows not only the largest integrated intensity but also the narrowest full-width at half-maximum (FWHM) for nc-Si. The narrower FWHM means a larger Si crystal size, and the corresponding size in sample FA-1000 can be estimated to be about 3 nm in diameter [9, 11]. In addition, the highest f_c of 76.8% is obtained from sample FA-1000. Hence, our results show that annealing temperature has a great effect on the crystallization of a-Si nano-clusters. Since the crystalline property of ZnO matrix has strong influences on the optical and electrical properties of the ZnO thin films [12], the XRD pattern of sample FA-1000 is examined and shown as inset of Fig. 2(b). The ZnO(0002) orientation located at 34.45° is clearly observed in sample FA-1000. In other

words, the high crystallinity of Si nano-clusters can form in the crystalline ZnO matrix by utilizing a ZnO/Si ML deposition structure with annealing temperature of 1000°C.
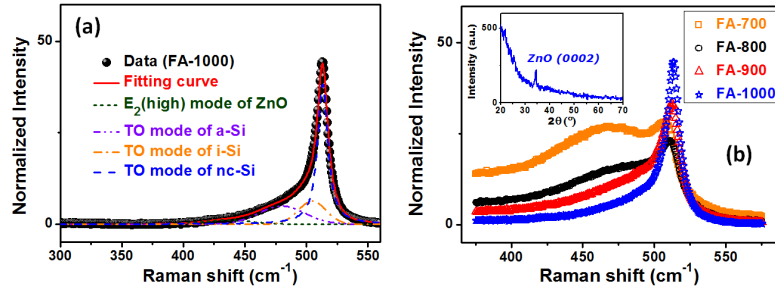

Fig. 2. (a) The curve-fitting result of Raman spectrum for sample FA-1000. (b) Raman spectra of the ZnO/Si ML thin films under different annealing temperatures. Inset shows the XRD pattern for sample FA-1000.

Table 1. Parameters of the Curve-Fitting Results in Raman Spectra for Nc-Si Phase and the Calculated Crystalline Volume Fraction of Si under Different Annealing Temperatures.

| Sample ID | TO mode of nc-Si phase | | | Crystalline volume fraction of Si (%) $f_c = (I_{i\text{-}Si} + I_{nc\text{-}Si})/(I_{a\text{-}Si} + I_{i\text{-}Si} + I_{nc\text{-}Si}) \times 100\%$ |
	Peak position (cm^{-1})	FWHM (cm^{-1})	Integrated intensity (a.u.)	
FA-700	/	/	/	25.0
FA-800	511.8	12.0	107.4	32.8
FA-900	512.6	11.9	338.5	58.9
FA-1000	513.2	10.0	583.2	76.8

Figures 3(a) and 3(b) shows the cross-sectional HRTEM images of the as-deposited and 1000°C-annealed ZnO/Si ML thin films for further understanding of the nano-structural properties. The ZnO/Si ML structure can be clearly observed after deposition from inset of Fig. 3(a) and is well maintained after annealing shown as inset of Fig. 3(b). The nano-scaled rough morphology different from that of the ML structures using Si-based dielectric materials as matrix [13] originates from the slight crystallization of ZnO thin-layers during deposition [14]. From Fig. 3(a), we can see the formations of a-Si nano-clusters with a size distribution of 3~5 nm separated by ZnO thin-layers after deposition. And a large number of nano-crystalline clusters marked in red dashed circles are found after annealing from Fig. 3(b). Combined with the Raman and XRD results, these nano-crystalline clusters are composed of the nc-Si QDs embedded in the crystalline ZnO matrix. Moreover, the observed size distribution of a-Si nano-clusters is well consistent with the examined height of nano-clusters in AFM image and the estimated average crystalline size of Si in Raman spectrum for sample FA-1000, and such size is proper to produce the quantum confinement effect for electro-optical devices integrating nc-Si QDs [1–3]. Therefore, we verify that the ZnO thin film with the suitable size of nc-Si QDs can be realized after furnace annealing.

The optical properties of the ZnO thin film with nc-Si QDs are also investigated and discussed. Figure 4 shows the PL spectra of sample FA-1000 and pure ZnO thin film with equal ZnO thickness of 105 nm under an identical annealing condition as a reference sample. The visible PL emission (PL$_{VIS}$) with a wide FWHM is observed in the pure ZnO thin film. Similar results have been reported and shown this PL$_{VIS}$ is from the contribution of the native defects in ZnO, which can be efficiently controlled by various post-annealing methods [15, 16].
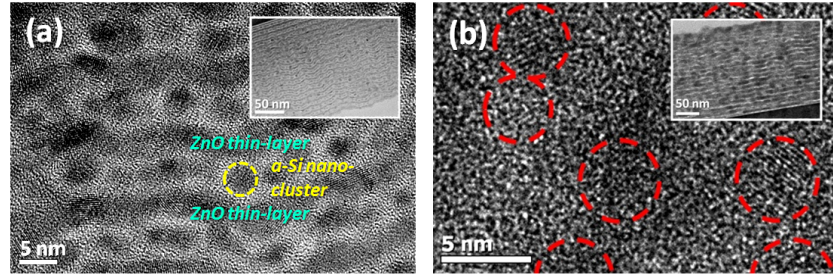
Fig. 3. The cross-sectional HRTEM images of the (a) as-deposited and (b) 1000°C-annealed (sample FA-1000) ZnO/Si ML thin films. Insets show the corresponding overall images.

Hence, the increased PL_{VIS} in sample FA-1000 can be mainly inferred from the higher native defect density in ZnO matrix since it has a smaller crystalline size than that in pure ZnO thin film. In addition to the increased PL_{VIS}, the PL spectrum accompanies increased near-infrared emission (PL_{NIR}) and an unusual peak ($PL_{unusual}$) located at 685 nm (1.81 eV), which have not been reported in pure or doped ZnO materials [15, 16], for sample FA-1000. This $PL_{unusual}$ may be contributed from the nc-Si QDs embedded in the ZnO matrix with wide bandgap. Because of the quantum confinement effect [17], an effective bandgap of nc-Si QD larger than the bandgap of bulk crystalline-Si (1.12 eV) is formed. Therefore, the obvious PL_{NIR} may be primarily resulted from the interface states between nc-Si QDs and ZnO matrix. Similar results have also been observed for nc-Si QDs embedded in SiO_2 matrix [18, 19]. For annealing temperatures lower than 1000°C, the PL_{VIS} and PL_{NIR} clearly dominate the PL emission properties and no obvious $PL_{unusual}$ peak is observed. This indicates the native defects in ZnO matrix and the interface states between Si QDs and ZnO matrix are excessively formed because of the lower crystal quality of Si QDs and ZnO matrix under lower annealing temperatures.
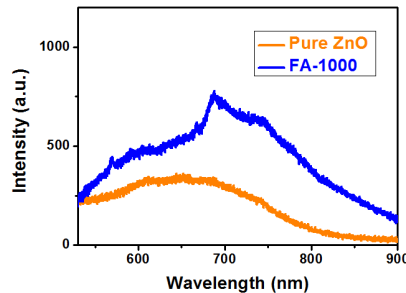

Fig. 4. PL spectra of sample FA-1000 and pure ZnO thin film after annealing at 1000°C.

To confirm the contributions of nc-Si QDs in PL spectrum and their impact on the optical properties of ZnO thin film with nc-Si QDs, the UV-VIS-NIR spectra are examined. Figures 5(a) and 5(b) show the light transmission, reflection, and absorption spectra of sample FA-1000 and pure ZnO thin film for comparison. For sample FA-1000, a high transmittance (T) in the long-wavelength range of 650 to 1000 nm and a high absorption in the short-wavelength range under 380 nm similar to general ZnO thin film are observed, and the T is higher than that of pure ZnO thin film owing to the reduced reflectance (R) resulted from the nano-scaled rough surface of sample FA-1000. The average R of sample FA-1000 (~9.5%) is significantly lower than that of pure ZnO thin film (~22.0%) in the measured wavelength range of 320~1000 nm. The sharp R peak occurred at the absorption edge of 380 nm in pure ZnO thin film originates from excitonic resonant emission, which is usually observed in the high-temperature annealed or epitaxial ZnO thin films [20, 21]. The T of sample FA-1000 obviously reduces with decreasing wavelength in the middle-wavelength range of 380 to 650 nm. At the same time, an increased absorbance (A) compared to pure ZnO thin film is

observed in the corresponding wavelength range. The increase of light absorption causes the decrease of light transmission in the middle-wavelength range because of the presnece of nc-Si QDs. To further verify the contributions of nc-Si QDs, Fig. 5(c) shows the PL spectrum and Tauc plot for the indirect allowed transition since the optical transition process in nc-Si QD system is dominated by a phonon-assisted mechanism [17]. The average indirect optical bandgap ($E_{g,opt.}$) can be evaluated by linear extrapolating the interception at the energy axis ($\alpha h\nu = 0$) from the plot of $(\alpha h\nu)^{1/2}$ as a function of incident photon energy ($h\nu$), where α is the optical absorption coefficient. The evaluated indirect $E_{g,opt}$ for sample FA-1000 is 1.86 eV, which quite matches the $PL_{unusual}$ peak energy (1.81 eV). Thus, we show that the nc-Si QDs embedded in ZnO matrix induce a sub-bandgap formation and in turn contribute the $PL_{unusual}$ and significant light absorption enhancement in the middle-wavelength range. Other than Si-based dielectric materials [22, 23], we successfully demonstrate the ability of sub-bandgap formation in ZnO material utilizing nc-Si QDs. Moreover, the $E_{g,opt.}$ of ZnO matrix can be obtained from the Tauc plot for direct allowed transition shown as inset of Fig. 5(c). The bandgap of 3.34 eV well agrees with that of general ZnO thin films [24]. These measurement results indicate that the ZnO matrix in sample FA-1000 still reserves its essential and advantageous optical properties even though the nc-Si QDs are embedded [24]. The realization of high crystallinity of Si QDs embedded in the crystalline ZnO matrix with a meaningful sub-bandgap provides a new and potential composite material for the development of future electro-optical devices.
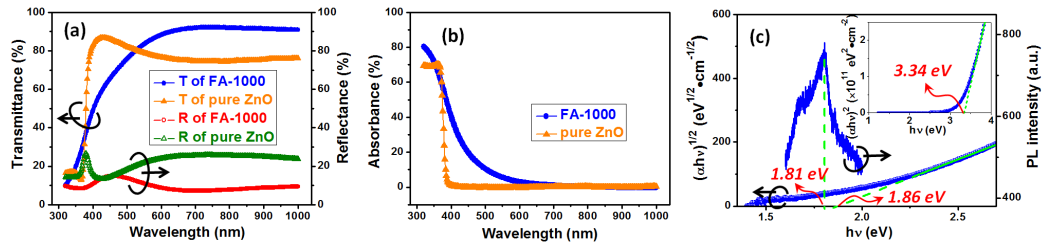

Fig. 5. (a) Transmission, reflection, and (b) absorption spectra of sample FA-1000 and pure ZnO thin film on quartzes. (c) PL spectrum and Tauc plot for indirect allowed transition of sample FA-1000. Inset shows the Tauc plot for direct allowed transition of sample FA-1000.

4. Conclusion

In summary, we had successfully fabricated the ZnO thin film with nc-Si QDs using a ZnO/Si ML structure with a post-annealing process. Our results indicate that 1000°C annealing temperature can result in highest crystallinity of Si QDs embedded in crystalline ZnO matrix. Though embedded with nc-Si QDs, the optical properties of ZnO thin film can be preserved in the long- and short-wavelength ranges. In the middle-wavelength range, the significantly enhanced light absorption owing to nc-Si QDs is obtained. In addition, an optical sub-bandgap of 1.86 eV closes to the unusual PL emission peak located at 1.81 eV is observed. These results represent the sub-bandgap formation in ZnO thin film by utilizing nc-Si QDs while maintaining the essential optical properties of ZnO matrix. We believe this novel composite material integrating ZnO thin film with nc-Si QDs has great potential for the future electro-optical device applications.